# Band-notched UWB Annular Slot Antenna with Enhanced Bandwidth by using EBG Via Holes

Ayman Ayd R. Saad, Deena A. Salem, and Elsayed Esam M. Khaled

***Abstract*—**In this paper, a design of a proximity-fed planar annular slot antenna with standard band-notched characteristic for ultra-wideband (UWB) applications is demonstrated. The band-notch is realized by nearly a half-wavelength split-ring parasitic element printed around the radiating patch. The patch is excited via a proximity-fed strip line with an arrangement of EBG via holes. The voltage standing wave ratio (VSWR) of the proposed antenna is less than 2.0 in the frequency band from 2.82 to 10.74 GHz, while showing a very sharp band-rejection performance at 5.51 GHz which preserved for IEEE 802.11a and HIPERLAN/2 services. The antenna is designed, simulated, and implemented. Measured data and simulated results show good agreements along with equivalent circuit results which obtained using Vector Fitting technique. The proposed antenna provides good gain flatness, high efficiency and omnidirectional field pattern over its whole frequency band excluding the rejected band. The results show that the proposed antenna is suitable for UWB applications.

***Keywords***—proximity-fed, slot antenna, ultra-wideband, band-notched, equivalent circuit, vector fitting

## I. INTRODUCTION

ULTRA-WIDEBAND (UWB) antennas designs are increased substantially since the Federal Communication Commission (FCC) in USA allow using the 3.1-10.6 GHz band for UWB communication [1]. The use of the 5.15–5.825 GHz band that is limited by IEEE 802.11a standard for wireless LAN systems causes a frequency interference with some UWB applications which share parts of the same spectrum. To prevent such interference a band-notch filter in the UWB system is necessary. Adding a filter to the UWB system increases the complexity of the system. A better design of the system is to have a frequency band-notch characteristic provided by the UWB antenna itself. Several UWB antennas with band-notched characteristic have been reported [2]-[10].

A. A. R. Saad is with the Electrical Engineering Department, South Valley University, Qena, Egypt (e-mail: dem_as@yahoo.com).

D. A. Salem is with the Electronics Research Institute, Giza, Egypt (e-mail: deenasalem3@ieee.org),

E. E. M. Khaled is with the Electrical Engineering Department, Assiut University, Assiut, Egypt (e-mail: esamk54_2000@hotmail.com).

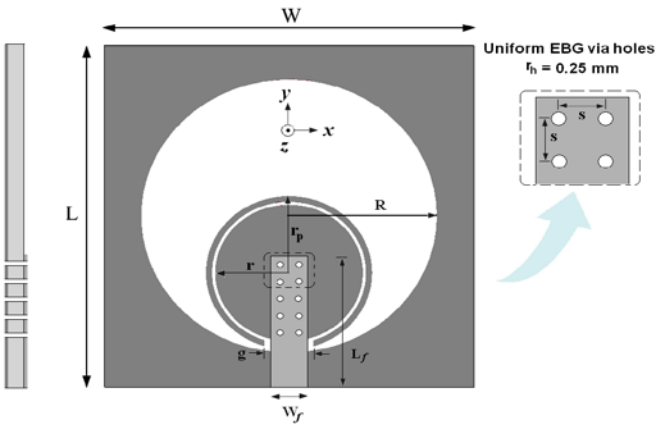


Fig. 1 Geometry of proposed planar annular slot antenna with split-ring parasitic element (L = 30 mm, W = 30 mm, R = 12 mm, r = 6 mm, $L_f$ = 11.5 mm, $W_f$ = 3 mm, $r_p$ = 6.75 mm, g = 4.0 mm, $r_h$ = 0.25 mm, s = 1.5 mm).

In this paper a simple annular slot antenna based on proximity-feeding technique with an arrangement of EBG via holes having band-notched characteristic for UWB applications is adopted. A band-notch filtering at 5.51 GHz is achieved by inserting a split-ring parasitic element around the radiating patch of the antenna. The performance of the proposed antenna is confirmed by simulation and measurement results. Details of the antenna structure and design methodology are described in Section II. Design results of the proposed antenna parameters and characteristics are obtained and discussed in Section III. The equivalent circuit of proposed antenna is synthesized in Section IV. This work is concluded with a brief summary in Section V.

## II. ANTENNA DESIGN AND STRUCTURE

Based on several parametric studies, the optimized antenna is designed as depicted in Fig. 1. The prototype antenna is fabricated on a 30 (L) x 30 (W) $mm^2$ FR4 substrate with relative permittivity 4.7, a loss tangent tan δ = 0.02, and a thickness h = 1.5 mm. A circular radiating patch of radius r = 6.0 mm is placed non-concentrically inside a circular slot of radius R = 12.0 mm etched off the ground plane. This circular slot represents a ground plane aperture (GPA). The centers of the circular patch and the circular GPA are on the same vertical symmetric line of the substrate. The distance between the lower edge of the circular patch and the lower edge of the circular slot is 1.0 mm. The circular patch is excited using a

50 Ω proximity-feed microstrip line placed on the other side of the substrate, with width $W_f$= 3.0 mm and length, $L_f$ = 11.5 mm [11]. A photograph of the implemented prototype antenna is shown in Fig. 2(a).

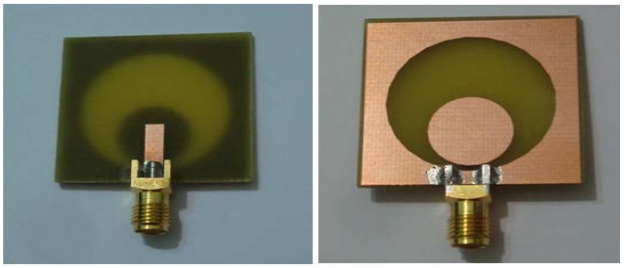

Front-view Back-view

(a)

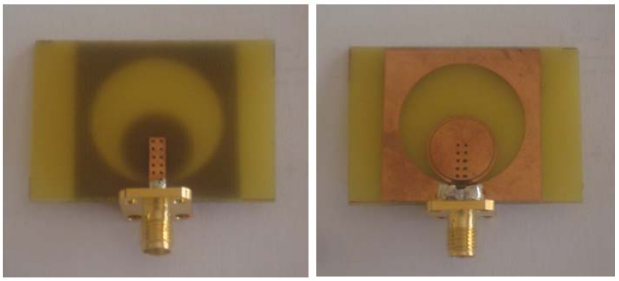

Front-view Back-view

(b)

Fig. 2 Photograph of the implemented antennas. (a) Prototype antenna. (b) Proposed antenna with EBG via holes and split-ring parasitic element

To enhance the impedance bandwidth of the specified prototype antenna ten circular electromagnetic band gap (EBG) via holes of radius $r_h$ = 0.25 mm are connecting the radiating patch and the microstrip feed-line through the substrate to achieve high magnetic coupling between the microstrip feed line and the radiating patch. The vertical distance between the centers of consecutive holes is s = 1.5 mm. A strip of width 0.5 mm is considered around the holes to the left, upper, and right edges of the microstrip line. To achieve the band-notch performance a split-ring parasitic element of external radius $r_p$ = 6.75 mm and with uniform width of 0.5 mm is inserted around the patch with a uniform separation of 0.25 mm between the patch and the parasitic ring. As shown in Fig. 1 a gap g = 4.0 mm is left between the two ends of the split-ring to fit the band-notch. A photograph of the implemented proposed antenna with EBG via holes and split-ring parasitic element is shown in Fig. 2(b).

## III. Results and Discussions

The proposed antenna is simulated and fabricated. The VSWR characteristics are measured using an Agilent HP8719 network analyzer. Fig. 3 shows the measured and simulated VSWR characteristics for the optimized dimensions for different cases of antenna design; without and with the EBG via holes, and with the split-ring parasitic element. The measured data agree well with the simulated results over the frequency band of interest. The measured VSWR characteristics of the prototype antenna range from 2.85 to 7.95 GHz for VSWR ≤ 2 which is less than the frequency spectrum (3.1–10.6 GHz) allocated by FCC for UWB communication. It is apparent that, the bandwidth of the prototype antenna is more enhanced by using the EBG via holes which ranges from 2.85 to beyond 14 GHz for VSWR≤ 2 that satisfy the UWB spectrum. Also, Fig. 3 shows that the split-ring parasitic element achieves a sharp band rejection at frequency 5.51 GHz that is suitable to avoid a frequency interference with the existed narrowband services such as IEEE 802.11a and HIPERLAN/2.

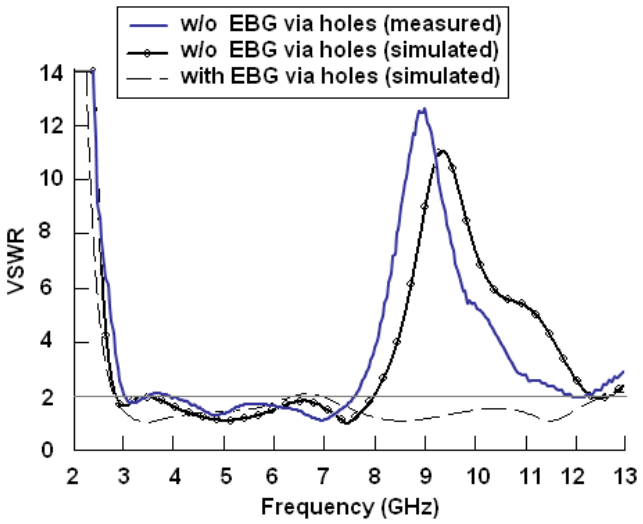


(a)

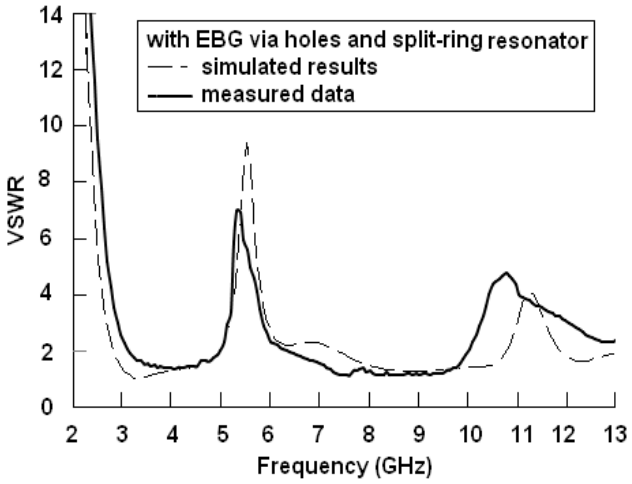


(b)

Fig. 3 Simulated and measured VSWR characteristics versus frequency for the proposed antenna. (a) With and without EBG via holes. (b) With EBG via holes and split-ring parasitic element.

Fig. 4 illustrates the effects of the parameters of the EBG via holes on the prototype antenna bandwidth. Fig. 4(a) shows the VSWR characteristics versus frequency for various numbers of holes. It is observed that as the number of EBG via holes increases the bandwidth of the antenna increases as

well. Fig. 4(b) shows the effects of the radius of the uniform holes on VSWR characteristic. As the radius of the holes increases the bandwidth increases. Fig. 5 shows the input impedance of prototype proposed antenna with and without EBG via holes (without the split-ring resonator). It is apparent that the input impedance of the proposed antenna with EBG via holes is more adjusted and better than that of the antenna without the EBG holes.

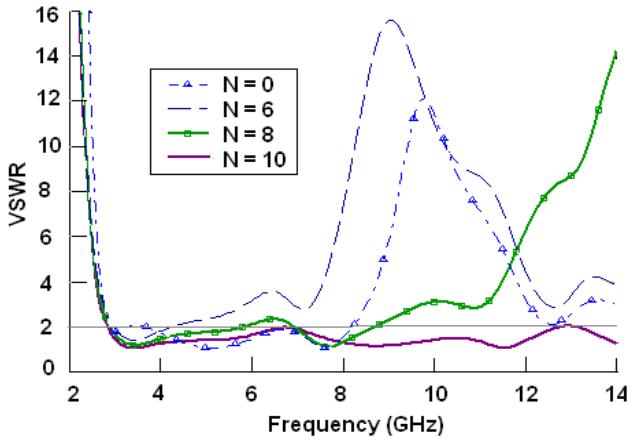


(a)

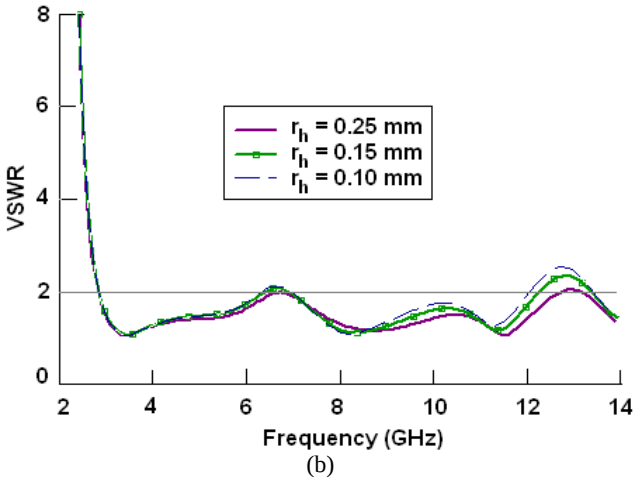


(b)

Fig. 4. Simulated VSWR characteristics versus frequency for the proposed antenna with EBG via holes and without the split-ring parasitic element. (a) For different numbers of holes. (b) For different holes radius.

The parameters of the split-ring parasitic element are analyzed in terms of the notch frequency and bandwidth. Fig. 6 shows the VSWR characteristic versus frequency with different external radius $r_p$ and gap length g of the split-ring parasitic element. Fig. 6(a) shows that as $r_p$ increases the band-notch shifted toward the low frequencies and the antenna bandwidth decreases. Fig. 6(b) illustrates that as the g increases which means that the circumference length of the split-ring decreases, the notched band shifts toward the high frequencies. It is noticed that the bandwidth of the notch-frequency function can be easily tuned by adjusting the radius of the ring and the length of its gap. The electrical length of a split-ring parasitic element is approximately a wavelength at the center frequency of the band notch (5.51 GHz). This novel band-notched UWB antenna has the capability to provide easy tuning of the bandwidth with good and suitable band rejection function.

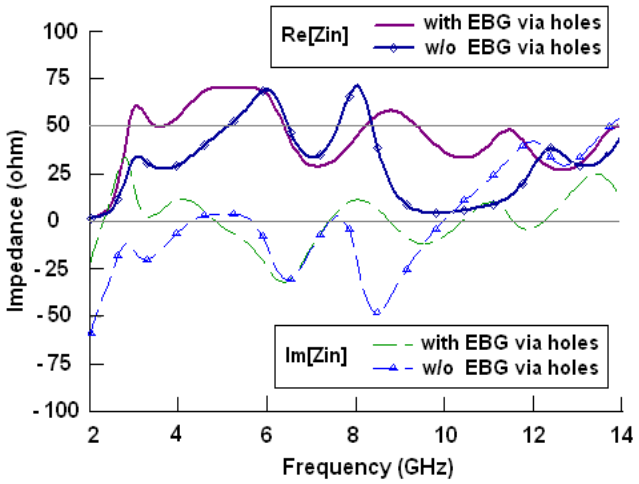


Fig. 5. Simulated input impedance of the prototype antenna versus frequency.

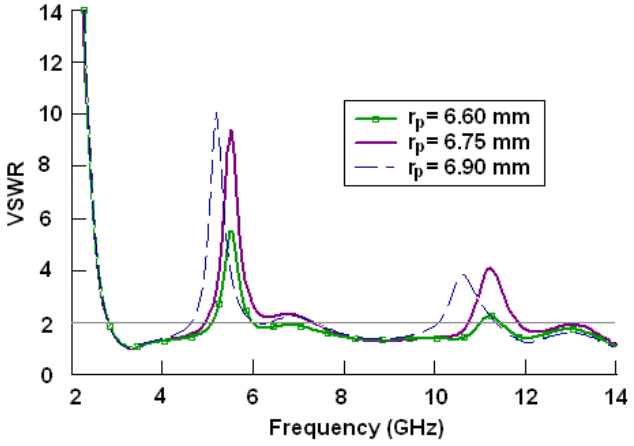


(a)

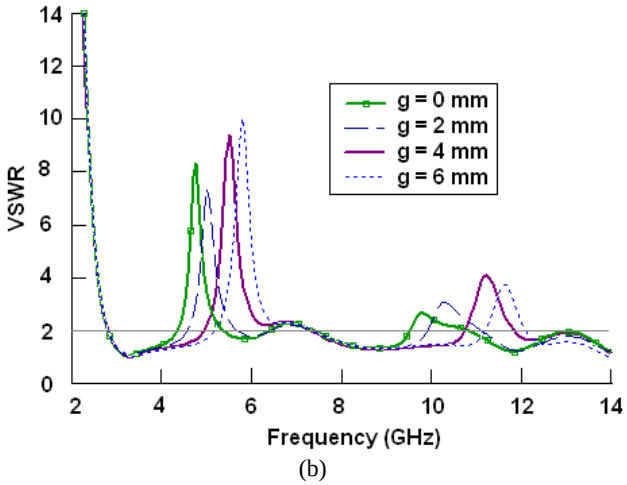


(b)

Fig. 6 Simulated VSWR characteristics versus frequency for the proposed antenna with the EBG via holes and with the split-ring parasitic element. (a) For different values of the split-ring external radius, $r_p$. (b) For different values of the gap length, g.

Fig. 7 shows the excited surface current distribution at the notch frequency of 5.51 GHz. As can be seen, there are dominant current flows on the split-ring strip and their direction is opposite with respect to the patch currents flow. This current distribution causes the antenna to be nonresponsive at the notch frequency.

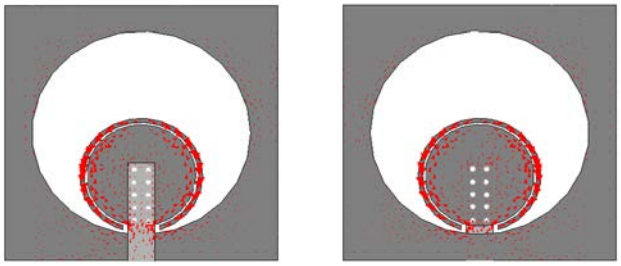

Front-view Back-view

Fig. 7 Simulated surface current distribution at the center rejected frequency 5.51 GHz for the proposed antenna with split-ring band-notch parasitic element.

The simulated radiation patterns of the proposed antenna in the *y-z* and *x-z* planes at frequencies 3.5 and 8 GHz are illustrated in Fig. 8. The radiation patterns are nearly omnidirectional in the *y-z* plane (E-plane), and quasi-omnidirectional in *x-z* plane (H-plane). The split-ring parasitic element has negligible effects on the radiation patterns of the antenna since both frequencies (3.5 and 8 GHz) are in the antenna pass bands. Fig. 9 presents the maximum gain of the proposed antenna with and without the band-notch function. The gain decreases drastically to nearly -8 dBi at the notched frequency band of 5.51 GHz. Stable antenna gain is achieved in the antenna's pass bands. From the simulation it is found that the radiation efficiency of this antenna is ranges from 76% to 95% overall the whole UWB frequency band, except for the notched band.

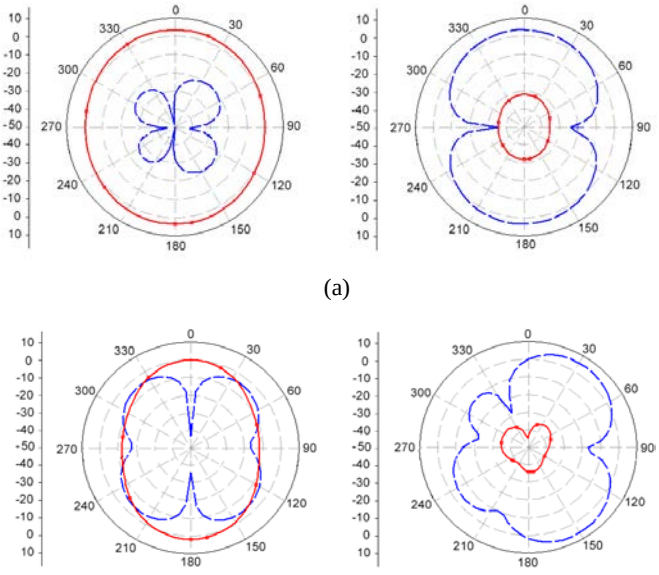

(a)

(b)

Fig. 8 Simulated radiation patterns of $E_\theta$ (dash line) and $E_\varphi$ (sold line) in the *y-z* and *x-z* planes for the proposed antenna at, (a) 3.5 GHz. (b) 8 GHz.

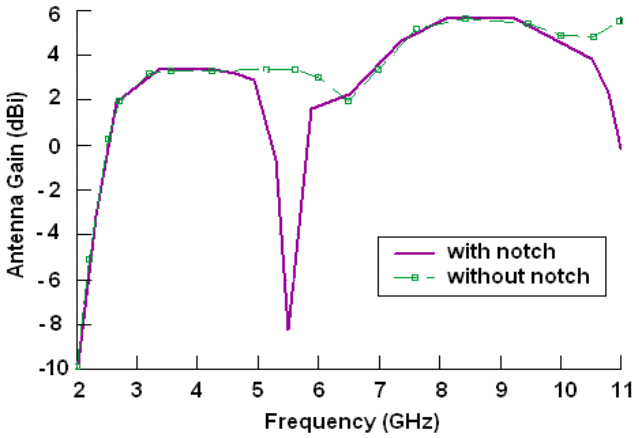


Fig. 9 Simulated antenna peak gain versus frequency for the proposed antenna with and without split-ring band-notch parasitic element.

## IV. EQUIVELANT CIRCUIT SYNTHESISED

For further comprehension of the proposed antenna performance, a SPICE–compatible circuit modelling method is applied. The method establishes the antenna lumped–element equivalent circuit model. The method is described as follows: First, obtain the simulated response of the input admittance or impedance of the proposed antenna in the frequency range of interest. There is no rule for the number of frequency points that should be sampled, but it is suggested to use no less than 100 points. Second, the simulated response of the input admittance is fitted by means of the Vector Fitting (VF) technique to obtain a rational function. Finally, the rational function is introduced into a SPICE–compatible equivalent circuit and the synthesized component values are obtained.

The rational function approximation of a certain frequency domain response $F(s)$ can be expressed as [12]:

$$F(s) = \sum_{k=1}^{N} \frac{res_k}{s - p_k} + d + se \tag{1}$$

where $res_k$ and $p_k$ denote the $k$–th residues and poles, respectively which are either real quantities or complex pairs (a complex number and its conjugate) of $N$ identical set of poles (order of approximation), $s = j\omega$ represents the complex frequency, and $d$ and $e$ are higher order coefficients (optional). All coefficients in (1) should be calculated so that an approximation of $F(s)$ is obtained over a given frequency interval. In general, VF solves this problem sequentially as a linear problem in two stages: poles identification and residues identification [12].

In the beginning, (1) is nonlinear since the unknown poles, $p_k$, are in the denominator. To convert this function into a linear one that could be solved with straightforward techniques, the poles are transformed into known quantities by giving them values at the beginning of the fitting process. These are called starting poles $\bar{p}_k$, and they exist only at the start of the evaluation. These starting poles allow, $res_k$, $d$, and $e$ to be obtained by linearly solving the matrix equation, $Ax =$

*B*, as described in [12]. After the first iteration, the starting poles are replaced by this new set of poles and $res_k$, *d*, and *e* are solved again and the process continues in an iterative manner depending on the number of iterations desired in the fitting. The details of this procedure can be found in [12].

After the final $p_k$, $res_k$, *d*, and *e* parameters have been obtained, these values are correlated to an equivalent circuit considers branches to represent either real poles or complex pairs poles or both. Only a specific modeling can consider branches to represent the equivalent circuit. When an equivalent circuit is created, the number of passive elements used is dependent on the order of the approximation.

Without loss of generality, *F*(*s*) is applied to be admittance–type function, *Y*(*s*) for the proposed antenna. The constant term *d* and the *s*–proportional parameter can be synthesized with a resistance, $R_0$, and a capacitance, $C_0$, respectively whose values are calculated as [13]:

$$R_0 = \frac{1}{d},\ C_0 = e \tag{2}$$

The equivalent circuit for the remaining part of $F(s) = \sum_{k=1}^{N} \frac{res_k}{s - p_k}$ can be evaluated as [13]:

– Equivalent Circuit for Real Poles:

Each real pole (for k = 1 to N) can be expressed as:

$$F(s) = \frac{res_k}{s - p_k} \tag{3}$$

Let us consider the series *RL* circuit represented in Fig. 10(a) to synthesized a function *F*(*s*) with a real pole. The *RL* admittance of a series *RL* circuit is:

$$Y_{RL}(s) = \frac{I(s)}{V(s)} = \frac{1}{R + sL} = \frac{\frac{1}{L}}{s + \frac{R}{L}} \tag{4}$$

Its pole and residue are:

$$p_k = -\frac{R_k}{L_k},\quad res_k = \frac{1}{L_k} \tag{5}$$

Given *N* set of poles and residues extracted by a fitting procedure, it is straightforward obtaining the corresponding couple of *R* and *L* parameters:

$$L_k = \frac{1}{res_k},\quad R_k = -\frac{p_k}{res_k} \tag{6}$$

– Equivalent Circuit for Complex Pole Pairs:

Let $res_1$, $res_2$, $p_1$ and $p_2$ be pairs of complex and conjugate residues and poles, respectively. The corresponding transfer function *F*(*s*) can be expressed as:

$$F(s) = \frac{res_1}{s - p_1} + \frac{res_2}{s - p_2} = \frac{(res_1 + res_2)s - (res_1 p_2 + res_2 p_1)}{s^2 - (p_1 + p_2)s + p_1 p_2} \tag{7}$$

Let us consider the *RLC* circuit represented in Fig. 10(b). It is a combination of a simple series *LR* circuit and a parallel *CR* circuit to synthesize a function *F*(*s*) with a complex pole pairs. The admittance of the combinational circuit can be written in terms of its residues and poles as:

$$Y_{RLC}(s) = \frac{I(s)}{V(s)} = \frac{1}{L}\frac{\left(s + \frac{1}{R'C}\right)}{\left(s^2 + \left(\frac{R}{L} + \frac{1}{R'C}\right)s + \left(\frac{R}{L}\frac{1}{R'C} + \frac{1}{LC}\right)\right)} \tag{8}$$

Compared with (7), the following correspondences can be established:

$$\begin{aligned} res_1 + res_2 &= \frac{1}{L} \\ -(p_1 + p_2) &= \frac{R}{L} + \frac{1}{R'C} \\ p_1 p_2 &= \frac{R}{L}\frac{1}{R'C} + \frac{1}{LC} \\ -(res_1 p_2 + res_2 p_1) &= \frac{1}{R'LC} \end{aligned} \tag{9}$$

The previous nonlinear set of equations can be solved in a closed form providing the following circuit parameters:

$$\begin{aligned} L &= \frac{1}{res_1 + res_2} \\ C &= \frac{res_1 + res_2}{p_1 p_2 + \left[-(p_1 + p_2) + \frac{res_1 p_2 + res_2 p_1}{res_1 + res_2}\right] \times \left[\frac{res_1 p_2 + res_2 p_1}{res_1 + res_2}\right]} \\ R &= \frac{1}{res_1 + res_2} \times \left[-(p_1 + p_2) + \frac{res_1 p_2 + res_2 p_1}{res_1 + res_2}\right] \\ R' &= -\frac{1}{C}\frac{res_1 + res_2}{res_1 p_2 + res_2 p_1} \end{aligned} \tag{10}$$

The procedures to extract such elements can be synthesized as described in [14].

The process can be started by $N = 2$ which is the minimum order of approximation. The complete synthesis SPICE–compatible equivalent circuit for input admittance of an antenna when $N = 2$ can provide either two real poles or one complex pair (a pole of order $N = 1$ is called a simple pole). Increasing the order of the approximation N will increase number of either the resultant real poles or the complex pairs. Only a specific modelling can consider branches to represent either real poles or complex poles or both.

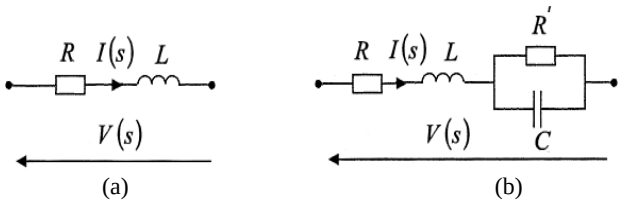


Fig. 10 (a) Equivalent *RL* circuit for real poles synthesis. (b) Equivalent *RLC* circuit for complex pair poles synthesis.

For the case of UWB antennas if the process is started with $N = 2$ the $Y(s)$ resulted will only fitted with one complex conjugate which causes that one of the resonance peaks being fitted. Because of the fitted resonance peaks depend on the location of the two starting poles, the resulting approximation for $Y(s)$ will be extremely inaccurate and the root-mean-square (rms) error becomes large. Increasing the set of initial poles will provide fitting for more resonance peaks. For the proposed antenna with EBG via holes and split–ring parasitic element the set of the initial poles is found to be 17 linearly spaced complex pairs ($N = 34$) and with 3 iterations to achieve a very accurate approximation fitting. The rational function approximation of $Y(s)$ using VF (poles and residues) is listed in Table 1. The fitting procedure provides 2 real poles and 16 complex conjugate pairs. Fig. 11 shows the magnitude and phase errors between the simulated results and the results using VF procedure. As clearly seen in Fig. 11, the proposed synthesis allows a satisfactory approximation of the input admittance, and the rms error on the magnitude is 1.6542e–005. Table 2 shows the component values for the equivalent circuit of the proposed antenna. Consequently, the equivalent circuit model for the input admittance of the proposed antenna for $N = 34$ is synthesized as shown in Fig. 12. The VSWR characteristics of the proposed antenna are shown in Fig. 13. Very good agreement between the simulated results and the equivalent circuit results along with the measured data is observed.

TABLE 1
THE RATIONAL FUNCTION APPROXIMATION OF THE INPUT ADMITTANCE Y(S) OF THE PROPOSED ANTENNA WITH EBG VIA HOLES AND SPLIT–RING PARASITIC ELEMENT

| Type and No. of poles | The Rational Function Approximation of $Y(s)$ | |
|---|---|---|
| | ***Poles*** (1e+11) | ***Residues*** (1e+8) |
| Real 1 | –0.0783 | 0.0685 |
| Real 2 | –1.2050 | –9.2022 |
| Complex 1 | –0.0036 ± 0.1453i | 0.7973 ± 0.1193i |
| Complex 2 | –0.0172 ± 0.2079i | –0.0002 ± 0.0008i |
| Complex 3 | –0.0439 ± 0.2165i | 0.6496 ± 0.2508i |
| Complex 4 | –0.0180 ± 0.2667i | 0.0012 ∓ 0.0005i |
| Complex 5 | –0.0527 ± 0.3351i | 0.3734 ∓ 1.4656i |
| Complex 6 | –0.0401 ± 0.3626i | 0.2905 ± 1.1645i |
| Complex 7 | –0.0142 ± 0.3951i | 0.0005 ∓ 0.0001i |
| Complex 8 | –0.0328 ± 0.4528i | 1.0448 ± 0.3480i |
| Complex 9 | –0.0140 ± 0.4985i | –0.0005 ∓ 0.0003i |
| Complex 10 | –0.0748 ± 0.5212i | 0.1319 ± 0.1038i |
| Complex 11 | –0.0050 ± 0.5906i | –0.0001 ∓ 0.0001i |
| Complex 12 | –0.0550 ± 0.6555i | 0.6972 ∓ 0.2632i |
| Complex 13 | –0.0122 ± 0.6778i | –0.0001 ∓ 0.0003i |
| Complex 14 | –0.0103 ± 0.7062i | 0.6840 ± 0.1279i |
| Complex 15 | –0.0559 ± 0.7895i | 1.1352 ∓ 0.0477i |
| Complex 16 | –0.0569 ± 0.9168i | 1.1789 ± 0.9457i |

$\boldsymbol{d}$ = 0.0096, $\boldsymbol{e}$ = 1.4425e–14

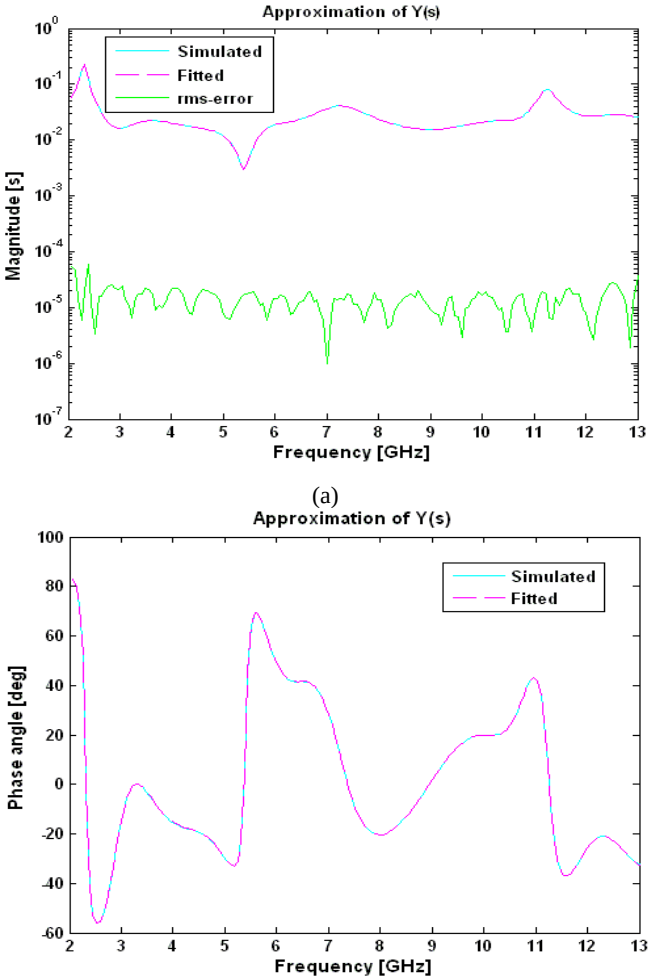


Fig. 11 Approximation of input admittance of the proposed antenna with EBG via holes and split–ring parasitic element. (a) Magnitude Functions. (b) Phase angles.

TABLE 2
SYNTHESIZED COMPONENT VALUES FOR THE PROPOSED ANTENNA WITH EBG VIA HOLES AND SPLIT–RING PARASITIC ELEMENT

| Type and No. of poles | The Equivalent Circuit Parameters | | | |
|---|---|---|---|---|
| | ***L*** (H) | ***R*** (Ω) | ***C*** (F) | ***R`***(Ω) |
| R1 | 1.4599e–007 | 1.1431e+003 | | |
| R 2 | –1.0867e–009 | –130.9469 | | |
| C1 | 6.2712e–009 | 15.8919 | 7.3876e–013 | –746.1545 |
| C 2 | –2.5000e–005 | 2036000 | –5.4438e–018 | –2.1642e+006 |
| C 3 | 7.6970e–009 | 98.1274 | 2.4122e–013 | –1.0446e+003 |
| C 4 | 4.1667e–006 | –3.8802e+004 | 2.8750e–016 | 2.6937e+005 |
| C 5 | 1.3390e–008 | –1.6906e+003 | 4.0538e–015 | 1.8033e+003 |
| C6 | 1.7212e–008 | 2.5708e+003 | 2.5889e–015 | –2.7328e+003 |
| C 7 | 1.0000e–005 | –6.4820e+004 | 6.1596e–017 | 1.7416e+006 |
| C 8 | 4.7856e–009 | 87.8722 | 9.1740e–014 | –923.6199 |
| C 9 | –1.0000e–005 | –313100 | –2.9589e–017 | 1.1854e+006 |
| C10 | 3.7908e–008 | 1.8384e+003 | 5.9970e–015 | –4.9722e+003 |
| C 11 | –5.0000e–005 | –2978000 | –2.8669e–018 | 5.9564e+006 |
| C 12 | 7.1715e–009 | –138.0220 | 2.8404e–014 | 1.1640e+003 |
| C13 | –5.0000e–005 | –1.0228e+007 | –1.1817e–018 | 4.1869e+006 |
| C 14 | 7.3099e–009 | 104.0579 | 2.6504e–014 | –3.0990e+003 |
| C 15 | 4.4045e–009 | 10.0097 | 3.6361e–014 | 3.0876e+003 |
| C 16 | 4.2412e–009 | 336.0533 | 1.7068e–014 | –863.4438 |

$\boldsymbol{R_0}$ = 90.9091 Ω, $\boldsymbol{C_0}$ = 1.4425e–14 F

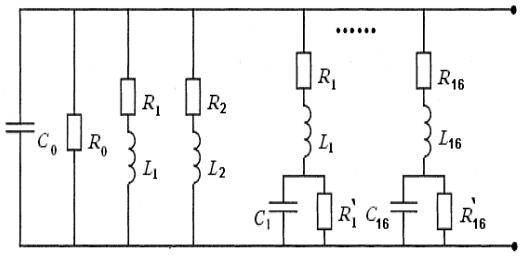


Fig. 12 Equivalent circuit synthesis of the proposed antenna with EBG via holes and split–ring parasitic element for $N$ = 34.

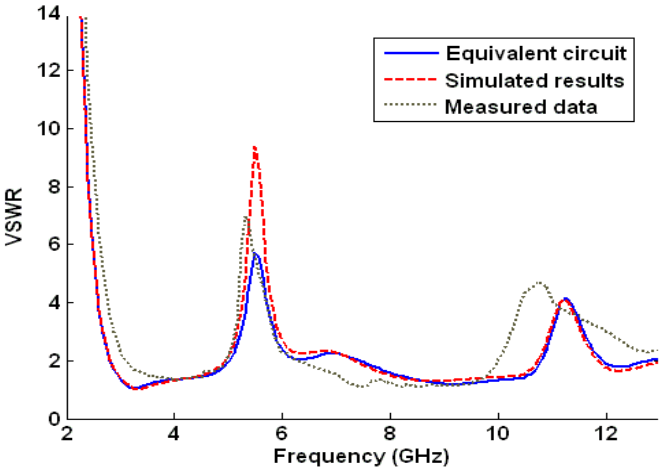


Fig. 13 VSWR characteristics as a function of frequency for the proposed antenna with EBG via holes and split–ring parasitic element.

It is noted that the VF technique guarantees stable poles and enforcing passivity. With stable poles and passivity enforced, the resulting equivalent circuit may still have unphysical circuit elements (negative resistance, capacitance and inductance), as shown in Table 2, even though we use low order of approximation. But we will never get an unstable simulation since the circuit as a whole will always consume power, whatever we connect to it [15]. However, numbers and values of the negative elements depended on the frequency range of the function to be fitted as well as the order of approximation used in that fitting. Higher accuracy can be easily involved by increasing the order of the approximation. But the complexity of the equivalent circuit will also be increased at the same time.

For instant, due to ultra–wide bandwidth, the resulting equivalent circuit may still have more negative circuit elements with large values, but the whole equivalent circuit will be passive. A circuit having negative capacitance/inductance can present, by duality, another inductance/capacitance element. In a negative capacitance the current will be 180° opposite in phase to the current in a positive capacitance. Instead of leading the voltage by 90° it will lag the voltage, as in an inductor. Therefore a negative capacitance acts like an inductance in which the impedance has a reverse dependence on frequency; decreasing instead of increasing like a real inductance. Similarly a negative inductance acts like a capacitance that has impedance which increases with frequency [16].

Finally, the major limitation of this approach is the fact that this technique is not systematic. In other words, the method does not contain a physics–based approach. Nevertheless, it is stressed that this technique can be used as a tool to aid engineers in designing an actual passive circuit that can be used to mimic the scattering parameter response of a UWB antenna [17]. In spite of this, good agreement between the simulated results and the fitted data with acceptable equivalent model behavior are obtained. The validity of the modeling method is verified and high accurate results are achieved. The provided circuit model is useful to consider the effect of the proposed antenna when integrated with the whole communication system. It also helps designers to predict the communication system performance.

## V. Conclusion

New and simple design of a band-notched UWB annular slot antenna with proximity-fed technique has been proposed and implemented. Electromagnetic Band Gap (EBG) via holes etched in the feeding line is used to improve the input impedance of the prototype antenna at high frequency bands. Band-notched characteristic is achieved by adding split-ring parasitic element around the radiating patch. The proposed antenna has a frequency band of 2.82-10.74 GHz for VSWR less than 2.0 with a rejection band at 5.51 GHz, which is complement with the IEEE 802.11a and HIPERLAN/2 services. The results show that the proposed design of the antenna with a band-notch function provides sufficient antenna performances such as, wide impedance bandwidth, suitable band rejection, high gain, and omnidirectional radiation pattern.

## References

[1] FCC, “Federal Communications Commission Revision of part 15 of the Commission’s Rules Regarding Ultra-Wideband Transmission System,” First Report and Order FCC, 02.V48, 2002.

[2] Y. Kim, and D. H. Kwon, “CPW-fed planar ultra-wideband antenna having frequency band notch function,” *Electron. Lett.*, vol. 40, no. 7, pp. 403–405, April 2004.

[3] S.-W. Su, K.-L. Wong, and C.-L. Tang, “Band-notched ultra-wideband planar-monopole antenna,” *Microw. Opt. Technol. Lett.*, vol. 44, no. 3, pp. 217–219, Feb. 2005.

[4] A. Kerkhoff, and H. Ling, “Design of a planar monopole antenna for use with ultra-wideband (UWB) having a band-notched characteristic,” in *Proc. IEEE AP-S Int. Symp. Dig.*, Columbus, OH, June 2003, vol. 1, pp. 830–833.

[5] E. S. Angelopouslos, A. Z. Anastopoulos, D. I. Kaklamani, A. A. Alexandridis, F. Lazarakis, and K. Dangakis, “Circular and ellipitcal CPW-fed slot and microstrip-fed antennas for ultrawideband applications,” *IEEE Antennas Wireless Prop. Lett.*, vol. 5, no. 1, pp. 294-297, 2006.

[6] J. Kim, C. S. Cho and J. W. Lee, “5.2 GHz notched ultra-wideband antenna using slot-type SRR,” *Electron. Lett.*, vol. 42, no. 6, pp. 315-316, March 2006.

[7] W. Choi, K. Chung, J. Jung, and J. Choi, “Compact ultra-wideband printed antenna with band-rejection characteristic,” *Electron. Lett.*, vol. 41, no. 18, pp. 990–991, September 2005.

[8] J. Qiu, Z. Du, J. Lu, and K. Gong, “A band-notched UWB antenna,” *Microw. Opt. Technol. Lett.*, vol. 45, no. 2, pp. 152–154, April 2005.

[9] R. Chair, A. A. Kishk, and K. F. Lee, "Ultrawide-band coplanar waveguide-fed rectangular slot antenna," *IEEE Antennas Wireless Prop. Lett*., vol. 3, no. 1, pp. 227-229, 2004.

[10] A. A. Kalteh, R. Fallahi, and M. G. Roozbahani, "5-GHz band-notched UWB elliptical slot antenna fed by microstrip line," in Proc. *Med. Microw. Symp.*, MMS 2010, Guzelyurt, August 2010, pp. 444–447.

[11] E. E. M. Khaled, A. A. R. Saad, and D. A. Salem, "A Proximity–fed annular slot antenna with different a band–notch manipulations for ultra–wideband applications," *Progress Electromagnetics Research B*, vol. 37, pp. 289–306, 2012.

[12] B. Gustavsen, and A. Semlyen, "Rational approximation of frequency domain responses by vector fitting," *IEEE Transactions on Power Delivery*, vol.14, pp. 1052–1061, July 1999.

[13] B. Gustavsen, "Computer code for rational approximation of frequency dependent admittance matrices," *IEEE Trans. Power Delivery*, vol. 17, no. 4, pp. 1093–1098, October 2002.

[14] G. Antonini, "SPICE equivalent circuits of frequency–domain responses," *IEEE Transactions on Electromagnetic Compatibility*, vol. 45, no. 3, pp. 502–512, August 2003.

[15] B. Gustavsen, and A. Semlyen, "Enforcing passivity for admittance matrices approximated by rational functions," *IEEE Transactions on Power System*, vol.16, pp. 97–104, February 2001.

[16] I. Hickman, *Analog Circuits Cookbook*, 2nd Ed., New York: Newnes, 1999.

[17] G. R. DeJean, and Manos M. Tentzeris, "The application of lumped element equivalent circuits approach to the design of single–port microstrip antennas," *IEEE Transactions on Antennas and Propagation*, vol. 55, no. 9, pp. 2472–2468, September 2007.